Journal Pre-proof

Environmentally Friendlier Wireless Energy Power Systems: The Coil on A Paper Approach

R. Brito-Pereira, N. Pereira, C. Ribeiro, S. Lanceros-Mendez, P. Martins

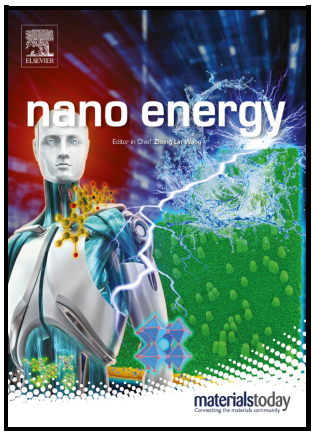

PII: S2211-2855(23)00228-8

DOI: https://doi.org/10.1016/j.nanoen.2023.108391

Reference: NANOEN108391

To appear in: *Nano Energy*

Received date: 7 July 2022
Revised date: 22 February 2023
Accepted date: 26 March 2023

Please cite this article as: R. Brito-Pereira, N. Pereira, C. Ribeiro, S. Lanceros-Mendez and P. Martins, Environmentally Friendlier Wireless Energy Power Systems: The Coil on A Paper Approach, *Nano Energy,* (2023) doi:https://doi.org/10.1016/j.nanoen.2023.108391

Environmentally friendlier wireless energy power systems: the coil on a paper approach

R. Brito-Pereira[a,b], N. Pereira[a], C. Ribeiro[a,c], S. Lanceros-Mendez[d,e] and P.Martins[a,f*]*

[a]Centre/Department of Physics, University of Minho, 4710-057 Braga, Portugal
[b]Centre for MicroElectroMechanics Systems (CMEMS), University of Minho, 4710-057 Braga, Portugal
[c]Centre of Biological Engineering, University of Minho, 4710-057 Braga, Portugal
[d]BCMaterials, Basque Center for Materials, Applications and Nanostructures, UPV/EHU Science Park, 48940 Leioa, Spain
[e]IKERBASQUE, Basque Foundation for Science, 48009 Bilbao, Spain
[f]IB-S Institute of Science and Innovation for Sustainability, University of Minho, 4710-057, Braga, Portugal

E-mail: *senentxu.lanceros@bcmaterials.net; pmartins@fisica.uminho.pt

Keywords: additive manufacturing, power transfer nanomodules: energy conversion and utilization; nanostructured materials for energy applications; green and sustainable science

Paper is ubiquitous in everyday life and a low-cost environmentally friendly material. Thus, the printing of advanced conductive/magnetic nanomaterials on paper will allow the scalable production of flexible smart electronics, including energy-storage devices, sensors, inductors or antennas, among others, contributing towards more sustainable electronics. Particularly, wireless charging technologies are becoming essential for internet-of-things (IoT)-related electronic devices due to the ever-decreasing dimensions of portable/mobile devices that limits the quantity of energy that can be stored.
Here, screen-printed paper-based coils and inductors operating on the 1 MHz - 20 MHz range are presented based on Poly(vynil alcohol)/Fe_3O_4 and Ag inks. The ability of the printed cores and inductors to be incorporated on flexible wireless power transfer modules (WPTM) is technologically demonstrated by wireless powering light-emitting diodes (LEDs). The achieved induction efficiency of 94% is the highest reported on printed WPTM.
The printed coils are also characterized by mechanical, hydrophobic and electrical properties that are suitable for IoT and industry 4.0 applications.

1. Introduction

There is a high interest in the use of natural polymers produced by or derived from living organisms (the so-called biopolymers) for electronic applications, principally triggered by increased sustainability concerns and widespread use of electronics [1-3]. Cellulose is the Earth's major available biopolymer, being also of large global economic significance [1, 4]. The possibility to integrate specific electronic purposes[5] within the production processing of the paper-based industry is consequently pivotal to enhance and expand the applicability of conventional cellulose-based papers [1, 6, 7] and a promising route to improve the flexibility of electronic materials[8, 9]. Paper can also decrease (in one order of magnitude) the carbon footprint of the printed circuit boards (PCBs) traditional substrates (such as epoxy and phenolic resins based on fossil feedstock: 5.7−7.6 kg CO_2.kg^{-1}) to 0.608 kg CO_2.kg^{-1}) [10, 11].
Mobility, supported by a variety of energy-storage technologies including rechargeable batteries and supercapacitors, has been a major market driver in the electronic industry, represented by hand-held devices, ubiquitous sensing, and wearable electronics[12-14]. Nevertheless, the ever-decreasing dimensions of portable/mobile devices, are increasingly

limiting the quantity of energy that can be stored [12, 15]. A solution to this contemporary technical challenge is the effect presented by Nicholas Tesla in 1907 [16]: the wireless electromagnetic energy transmission through wireless power transfer modules (WPTM) [17-20]. Such technology has been re-considered as a possibility to ensure a stable energy-supply for current and future mobile devices including small mobile electronics, wearable sensors, and implantable medical devices [21-23]. Further, such approach facilitates user convenience when combined with portable/mobile devices by eliminating wiring and connectors in power transfer systems [12, 17, 24]. Nevertheless, to be fully-framed into the current paradigms of increased sustainability and decreased environmental impact of materials and processes, additive manufacturing technologies and bio-based materials should be considered [6, 25, 26]. Additive manufacturing technologies are versatile and environmentally-friendlier, also allowing the design of customized structures (nanometric, asymmetric, flexible, or stretchable) that are essential for improved integration in a variety of applications[12, 27-29]. From the different additive manufacturing technologies, screen printing is a popular and matured technique that adds affordability, easiness, speed, and adaptableness to the production process, offering precise control over in transfer, excellent print resolution, and diversity on the substrate choice [30, 31]. Screen printing is also compatible with high viscosity inks (μ≈0.5-5 Pa.s), minimizing ink flow on the substrate after pattern deposition [27, 32, 33]. Further, screen printing technique can easily realize the preparation of paper-based devices with different patterns, being also uniform, fast and simple to scale up [34, 35].

Thus, in the scope of this technological scenario this work reports on screen-printed of Ag-based coils and Poly(vynil alcohol)-Fe_3O_4 cores on four commercially available papers and their use as wireless power systems.

PVA was selected as the magnetic core polymer binder since it is a water-soluble and biodegradable synthetic polymer, presenting good mechanical properties and biocompatibility [36-38]. Analogously Fe_3O_4 (FO) nanoparticles were chosen as magnetic component due to their high magnetic permeability and the possibility to be produced through environmentally-friendly approaches [39-41]. Once Ag-screen printed conductors offer a way to produce electronic devices in high quantities on flexible substrates with limited waste, suitable for high volume markets, DuPont ME603 Ag-based ink with a solid content between 49% and 53%, and sheet resistivity less than 200 mΩ sq^{-1}.mil^{-1}, it were used as conductive ink [12, 40, 42]. As a proof of concept, the first printed paper-based WPTM reported on the literature was fabricated and evaluated.

2. Materials and methods

2.1 Materials

Poly(vynil alcohol) (PVA) and Whatman nº1 cellulose paper (WCP) were purchased from *Sigma-Aldrich* (Missouri,USA), LUSTIGT origami paper (LOP) was purchased from IKEA (Delft, Netherlands), photo paper (PHP) was purchased from Epson (Suwa, Japan), A4 laser printing paper (A4PP) was purchased from Navigator (Setubal, Portugal). Fe_3O_4 (FO) nanoparticles (≈ 30 nm particle size) were purchased from *Nanoamor (Texas, USA),* DUPONT ME603 stretchable conductive silver ink was obtained from *DuPont* (Wilmington, USA).

2.2 Coil fabrication

First, FO nanoparticles were added (90 wt.%) to (4 mL, 6 mL, 8 mL and 10 mL) distilled water and 1g of PVA powder under mechanical agitation until all polymer being dissolved.

Different water quantities have been selected to tailor the viscosity of the ink for screen-printing[27]. The resulting mixture (PVA-FO) was screen printed in 8 layers over the four paper substrates. After the spreading step, the samples were put in a laboratory precision stove (JP Selecta, Model 2000208 – 10 minutes at 120°C), for complete removal of the water. Then, the printed substrates were removed from the oven and cooled down at room temperature (≈30 ºC) (**Figure 1 a**).

After the previous procedure, the stretchable conductive silver (Ag) ink was screen printed with a home-made system (with a vacuum table and adjustable speed for the printing squeegee rulers) over the samples, with a 120 wires polyester mesh, reaching a final thickness of ≈5 µm. For the printing process, a stencil with 550 × 450 mm frame dimensions placed at 3 mm distance of the substrate and a printing velocity of 0.3 $m.s^{-1}$ was used. After this step the paper-based WPTM (**Figure 1c-g**) were ready to be tested for IoT and Industry 4.0 related applications (**Figure 1h**).

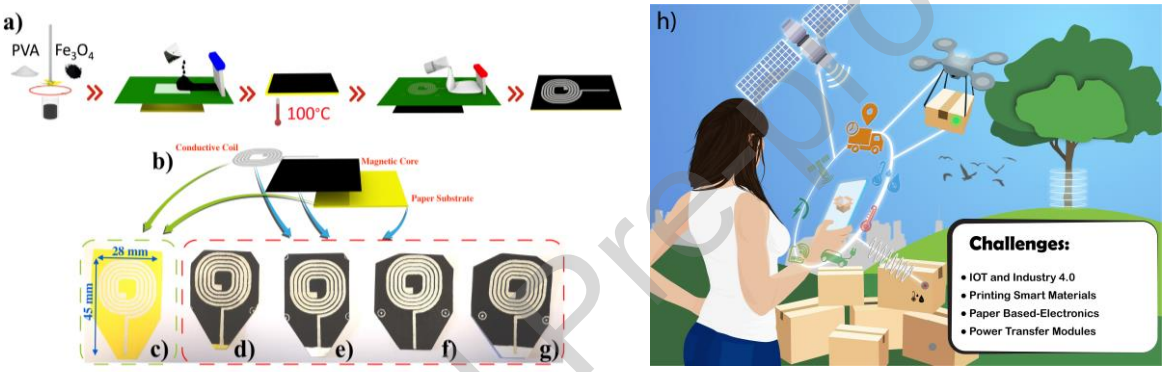

Figure 1 a) Scheme of the experimental procedure used to produce the WPTM. b) Schematic of the 3-layer coils. Photographs of the printed samples: c) LOP/Ag; d) LOP/PVA-FO/Ag, e) A4PP/PVA-FO/Ag, f) WCP/PVA-FO/Ag, and g) PHO/PVA-FO/Ag. h) Schematic representation of the technological scenario to which this work contributes.

The Ag ink was printed directly on LOP (c) and on papers with a previously PVA-FO printed layer, namely: d) LOP/PVA-FO/Ag, e) A4PP/PVA-FO/Ag, f) WCP/PVA-FO/Ag, and g) PHO/PVA-FO/Ag. In this way the latter samples were composed of a conductive Ag layer, a magnetic PVA-FO core, and a paper substrate.

2.3 Materials and device characterization

Rheology experiments were performed on AresG2 rheometer with a 40mm flat plate geometry and a 1 µm gap. The different mixtures were moved onto the rheometer plate immediately after the PVA dissolution and incorporation of the FO particles, avoiding any sedimentation. Flow curves have been acquired by a 3-shear rate sweeps program (up-down-up) in order to exclude the time-dependence, setting a nonstop ramp and a 0 to 300 s^{-1} shear rate. The apparent viscosity at 3 s^{-1} was studied from unsteady-state (curve 1) once for this condition the structure was less disturbed. All other shear rate values (steady-state) were evaluated from curve 3. The determined viscosity (η) values for the different mixtures were related at distinct shear rates (γ), supposing that the mixtures followed a power-law model [32, 43] (**equation 1**):

$$\eta = K\gamma^{N-1} \qquad \text{(equation 1)}$$

where the coefficients N and K can be experimentally determined.

The morphology of the developed materials was evaluated by scanning electron microscopy (SEM) using a NanoSEM - FEI Nova 200 (FEG/SEM) scanning electron microscope (10 kV). Before experiments, all paper-based samples were coated with Au on a Polaron SC502 sputter coater. The thickness of the layers was calculated from 5 images with 15 measurements in each image by using an ImageJ software.

The identification/quantification of the samples elements was performed with desktop SEM coupled with energy-dispersive X-ray spectroscopy (EDS) analysis (Phenom ProX with EDS detector + ProSuite software) purchased from Phenom-World BV, Netherlands, at 15 kV and spot size of 5.1. All samples were previously connected to Al substrates with electrically conductive carbon adhesives (obtained from PELCO Tabs™). Several locations were analysed for the final elemental composition.

Contact angle measurements on the different samples were performed using a Data Physics OCA20 instrument by the static sessile drop method with different mixtures (PVA-FO ink, Ag ink and water). For that, drop of 3 µL of the different liquids were left on the surface of each sample and the different contact angles were measured using the SCA20 software. The mean contact angle and standard deviation were calculated to each sample over the measurement at six different locations.

Adhesion of the printed inks was investigated with an adapted tape peel test [44] carried out on samples with a 1 cm x 1 cm size. Briefly an adhesive tape (3 M Scotch® Magic™ tape 810) was pressed on the surface of the printed samples with different forces (50N, 100N, 150N and 200N for 30 seconds using a Shimadzu AG-IS universal test set-up, in compression mode at $2mm.min^{-1}$. After that, the tape was removed from sample at the same velocity, while monitoring the force applied on the sample. The different samples were weighed before and after each test, to determine the mass loss in each printed coil.

The electrical characterization of the coils was executed on a Quadtech 1920 Precision LCR apparatus. The inductance change over frequency has been evaluated in the frequency range from 1kHz to 1MHz for the coils with and without a magnetic PVA-FO core. A Picoscope 2205A oscilloscope and a Agilent 33220A function generator were used for the energy transfer capibility evaluation. All coils exibited a similar electrical resistance (≈20 Ω measured with a Fluke 117 TRUE RMS multimeter).

The energy transfer capability of the printed inductors was studied as a function of the vertical distance (h), horizontal distance (w) and frequency in the 1MHz to 20MHz frequency range, that includes the standard frequency - 6.78 MHz - for resonant wireless power transfer modules[12] and the near field communication NFC frequency of 13.56 MHz [45]) .
The induction capability (IC) has been determined trought equation 2:

$$IC=(A_E/A_R)\times 100 \qquad \text{(equation 2)}$$

where A_E is the amplitude of the emited signal and A_R the amplitude of the received signal.

3. Results and Discussion

3.1 Materials evaluation

The ink viscosity for screen printing that allows to i) minimize the amount of the ink dispensed/transferred out of the mesh and to the substrate during screen printing process, ii) avoid the coffee ring effect, and iii) obtain an uniform deposition is on the 0.5 to 5 Pa.s range. Thus, evaluation of the rheological characteristics and the viscosity of the PVA-FO inks as a function of the volume of the water per gram of PVA was achieved as presented in **Figure 2**.

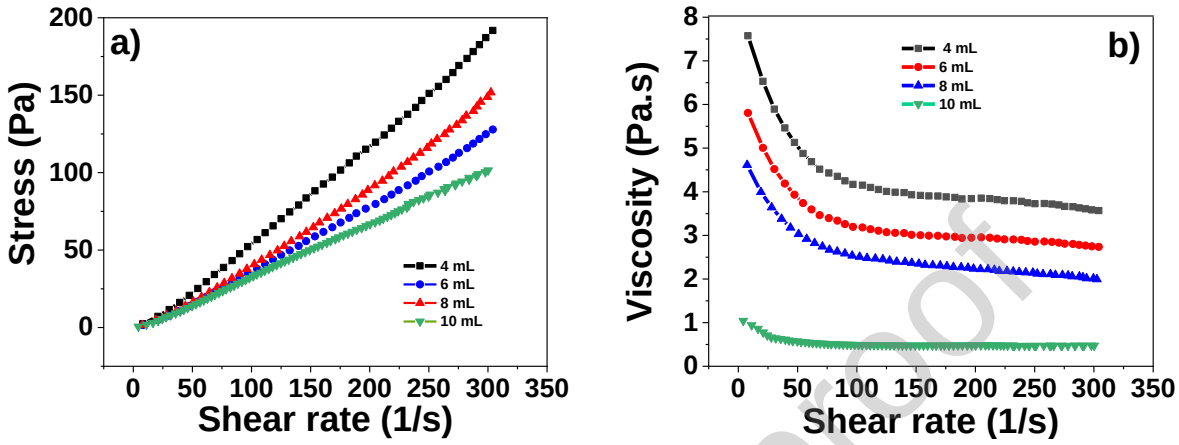

Figure 2. a) Shear stress versus shear rate of the different PVA-FO inks; b) viscosity values of the different PVA-FO inks as a function of the shear rate.

It is detected that as the shear rate values increases the shear stress values also increase, almost linearly. (**Figure 2a**) for all the developed inks. When the shear rate is applied, the ink components are reordered to accommodate the impact of the shear rate. The overall shear force is smaller for lower shear rates due to the slow response time of the inks: for the smaller shear rates the ink components have enough time to reorder, increasing the shear rates lead to insufficient reorganization times and higher induced stress [46]. It is also detected a higher slope in the samples with lower water content, resulting from the higher viscosity for those compositions. Thus, the viscosity as a function of the water content and shear rate (**Figure 2b**) shows the increase of the viscosity with decreasing water content, independently of the shear rate.

Based on the results of **Figure 2b**, the PVA-FO ink with 6 mL of water/ 1 gram of PVA has been selected to print the magnetic core of the inductor once the exhibited viscosities, in the 3 to 6 Pa.s range, are compatible with high quality screen prints [27]: such high-viscosity values favor amount of the ink transferred to the substrate and minimize the substrates' ink flow on after the screen-printing.

Aiming to optimize the PVA-FO and Ag ink spreading on the different commercially available paper substrates, essential for a successful printing [47, 48], and to verify under which conditions the printed coils were less permeable (high permeability can lead to the destruction of the PVA-FO layer once PVA is soluble in water), contact angle experiments have been performed (**Figure 3**).

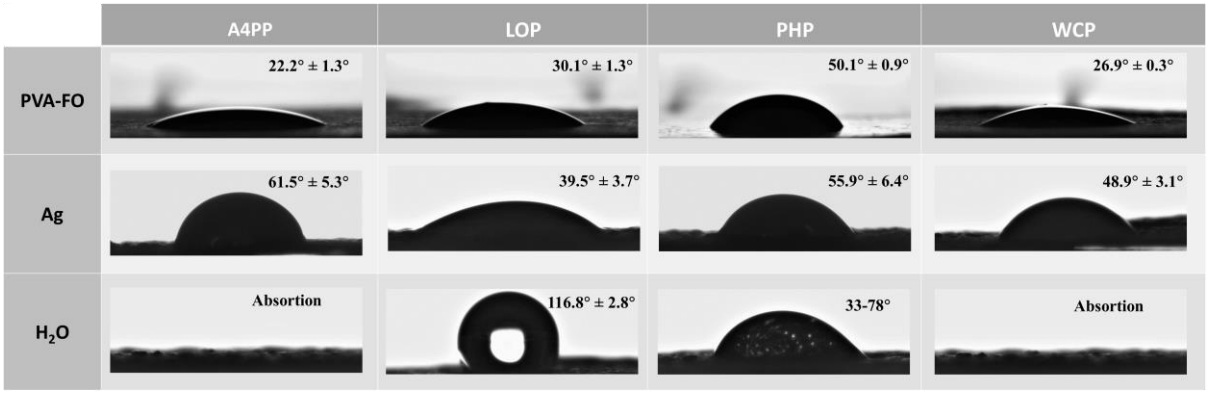

Figure 3. Contact angle at room-temperature of: first line- PVA-FO ink on the 4 paper substrates (A4PP, LOP, PHP, and WCP); second line- Ag ink on the 4 paper/PVA-FO substrates (A4PP/PVA-FO, LOP/PVA-FO, PHP/PVA-FO, and WCP/PVA-FO); third line: H_2O on the 4 paper/PVA-FO substrates (A4PP/PVA-FO, LOP/PVA-FO, PHP/PVA-FO, and WCP/PVA-FO).

The paper that exhibited the lowest contact angles combination (angle with PVA-FO ink + angle with Ag ink) was LOP (30.1º + 39.5º) that led to a stronger wetting, promoting a better drop spreading and printing quality [47, 49] of both layers. Smaller contact angles will result in overspill and overspreading of the ink, while larger contact angles could lead to the formation of mechanical instabilities and poor spreading [49]. The last line of **Figure 3** reveals that the paper which leads to improved hydrophobicity is also LOP, which will make this printed coil more stable when in contact with high humidity environments [50].

After, the room-temperature magnetic properties of the FO magnetic nanoparticles, the magnetic layer (PVA-FO) and the different paper/PVA-FO samples have been accessed by VSM measurements.

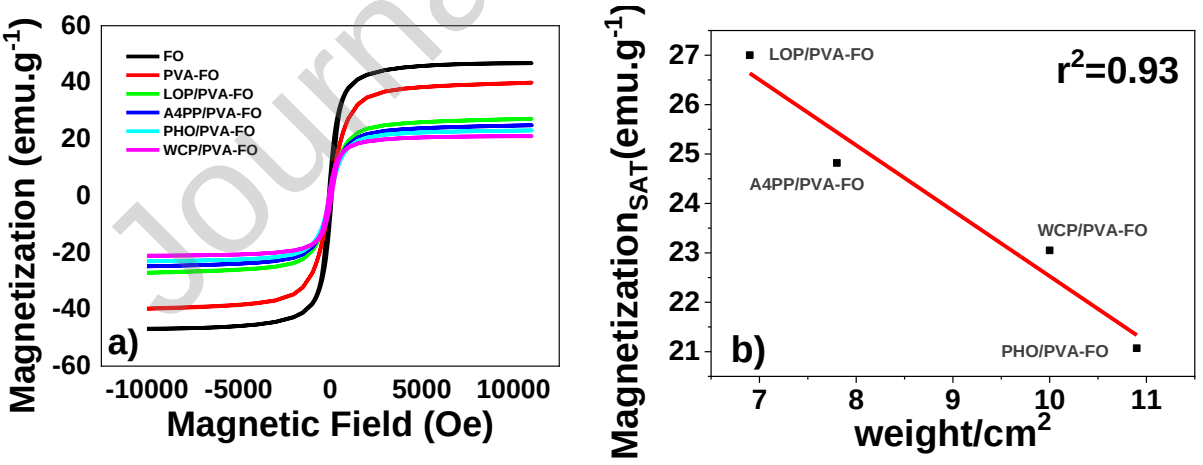

Figure 4. a) Magnetization at room-temperature vs applied DC magnetic field for different samples. b) Magnetic saturation ($Magnetization_{SAT}$) as a function of the weight/cm^2 of the different papers used in this study.

All FO-based samples show almost a complete absence of hysteresis, remanence, and coercivity consistent with the superparamagnetic behavior, once room temperature (≈25 °C) is above the blocking temperature and the nanoparticle's magnetic moment is able to rotate in response to the imposed DC magnetic field[6, 51]. Additionally, the magnetic saturation of the PVA-FO layer (≈40 emu.g^{-1}) that has 90 wt.% of FO corresponds to 87% of magnetic

saturation the pure FO (≈47 emu.g^{-1}), thus showing that the printing process did not substantially affect the wt.% of FO in the polymer matrix.
Finally, **Figure 4b** reveals that heavier papers lead to lower magnetic saturations because of the introduction of a greater amount of non-magnetic material for the paper-PVA-FO composite. The sample that exhibited the highest magnetic saturation was the LOP/PVA-FO (≈27 emu.g^{-1}).

In order to study the adhesion stability of the printed layers, peeling tests (**Figure 5**) have been performed on the coils printed in the different paper substrates.

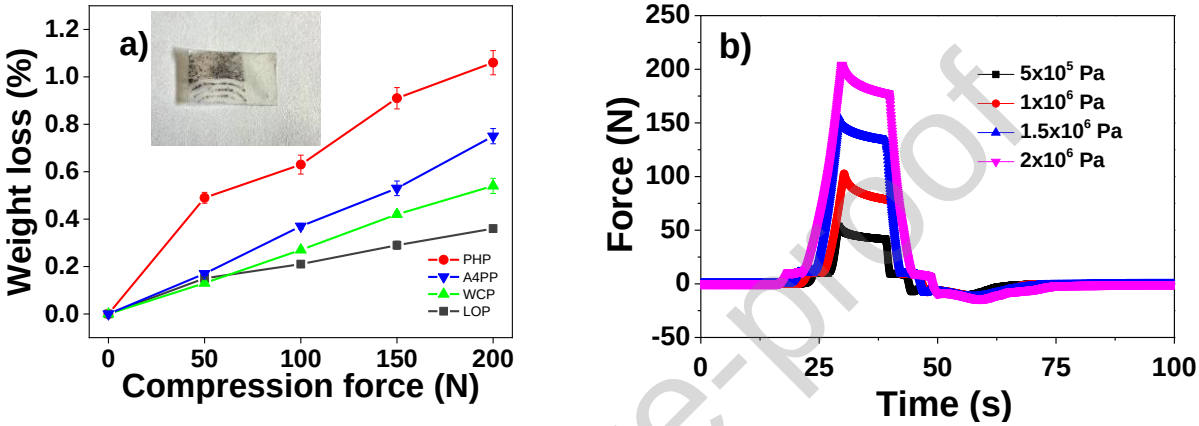

Figure 5. a) Weight loss for the different paper/PVA-FO/Ag samples as a function of the peeling force. The inset shows a representative piece of tape after a peeling test. b) Force profile of the peeling test for the LOP/PVA-CFO/Ag samples a function of time and pressure.

Figure 5a reveals that the weight loss increases with increasing compression force, being maximized for the sample with PHP (≈1%) and minimized for the sample with LOP (≈0.3%). The force profile during the peeling test for the LOP/PVA-CFO/Ag sample (**Figure 5b**) reveals that the highest compression force (200N) also leads to the highest peeling force (15N) and the lowest compression force (50N) leads to the lowest peeling force (10N), observations that explains the differences detected on **Figure 5a**. In a second round of tests, none of the samples experienced weight loss. The VSM analysis of the tape pieces used on the peeling tests revealed that all the material ripped out was from the PVA-FO layer. The Ms of the tape piece of Figure 5a's inset was ≈0.09 emu that corresponds to the magnetization of ≈ 2 mg of PVA-CFO. ≈ 2 mg was also the increment in the weight of the tape piece after the peeling test. The same strategy was applied to all tape pieces used in the peeling tests.

Figure 6 shows representative SEM cross-section images of the printed coils in different paper substrates, revealing an irregular shape with lumps and ridges.

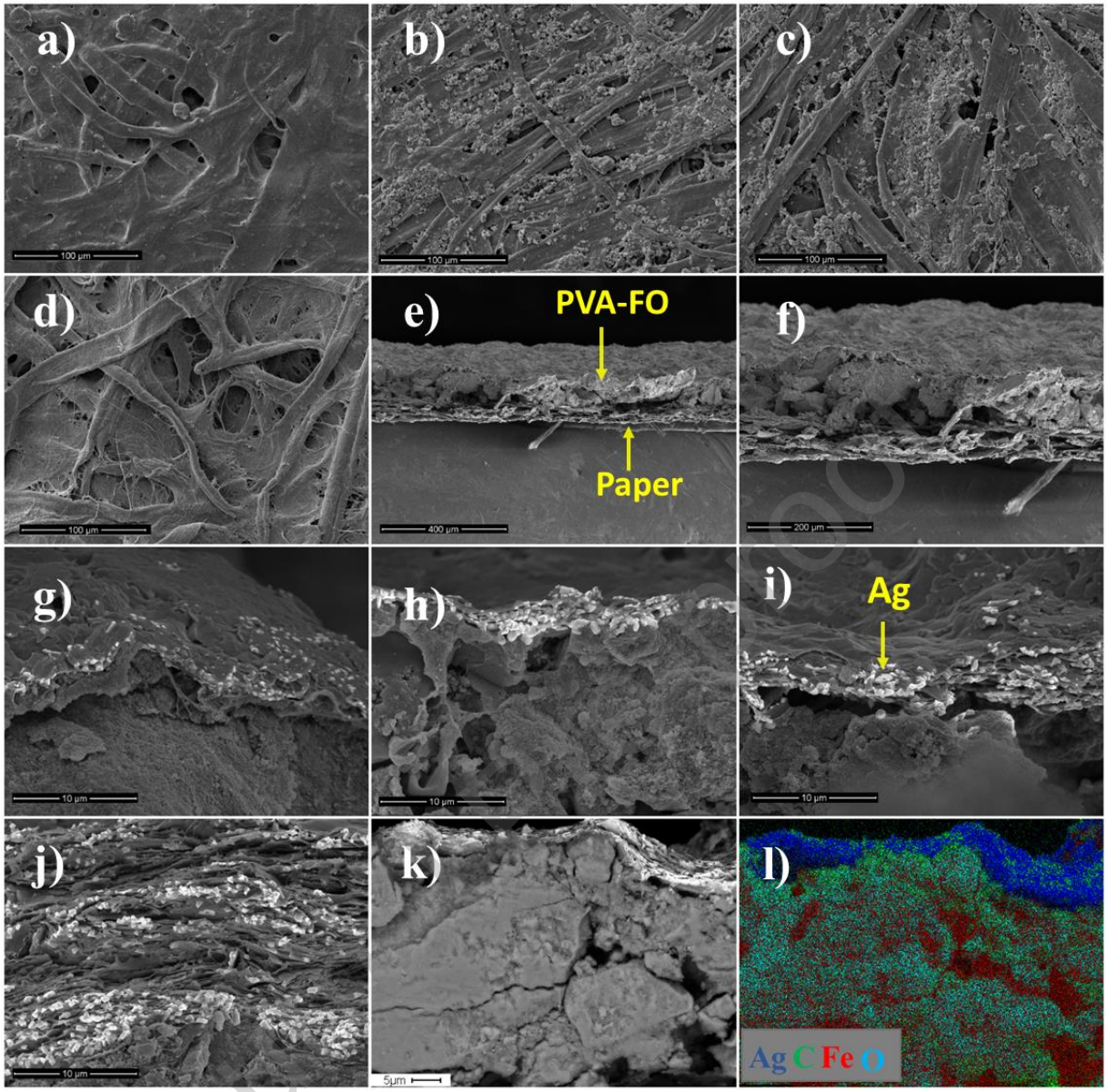

Figure 6. Characteristic surface SEM micrographs of the: a) LOP; b) A4PP; c) WCP, and d) PHP. Characteristic cross section SEM micrographs of the LOP/PVA-CFO/Ag coils (e-g) with different magnifications (e - 250x; f – 500x and g – 10000x). 1000x magnification cross section SEM micrographs for samples: h) A4PP/PVA-CFO/Ag; i) PHP/PVA-CFO/Ag, and j) WCP/PVA-CFO/Ag. k) Cross section SEM micrograph of the LOP/PVA-CFO/Ag coils on the site where the EDS mapping image was taken. l) EDS mapping image taken on the (k) site.

The surface SEM images of the papers used in this work (**Figure 6 a-d**), revealed the typical presence of fibers of cellulose-based materials [52]. Despite the common random fiber orientation, some differences are detected between a/d images and b/c images, that correspond to LOP/PHP and A4PP/WCP, respectively. LOP and PHP are characterized by less voids/pores, observation that is consistent with the lower wettability observed in **Figure 3** [53].

No significant differences can be found on the cross-section topographies of the different samples (even when submitted to the peeling tests). Additionally, and despite the high FO content (90 wt.%), magnetic nanoparticles seem to be uniformly distributed along the PVA-FO layer. The images with higher magnification (**Figure 6 g-k**) allow to detect the presence

of Ag (clearer structures) on the surface of the different laminates. SEM images also allow to verify that the different layers remained mechanically attached in layers that did not overlap, determining condition for each of them to correctly fulfill their function: paper: substrate; PVA-FO: magnetic core; and Ag: conductive line. From SEM images was also possible to obtain the thicknesses of all layers: LOP = 53 ± 4 µm; A4PP = 74 ± 5 µm; PHP = 85 ± 6 µm; WCP = 105 ± 8 µm; PVA-FO = 113 ± 10 µm; and Ag 3.8 ± 1.1 µm. Despite all samples been cut in liquid nitrogen all of them show distortions resulting from the cutting process.
The elemental mapping analysis (**Figure 6l**) confirmed the presence of magnetic nanoparticles (Fe locations) on the PVA-FO core and that the printing process ensures a uniform distribution, both in depth, length, and width. Finally, it is confirmed that the conductive Ag ink remains at the surface of the laminate.

After the previous results being obtained, the LOP/PVA-CFO/Ag coils were selected to carry out the energy transfer experiments (**Figure 7**), once it exhibited better printability, higher hydrophobicity, and suitable mechanical adhesion. The conductivity of the printed Ag lines was $\approx 1x10^{5}$ $S.m^{-1}$, and the dielectric constant ε' and the capacitance (C) of the PVA-FO core at 1 kHz were 27 and 1×10^{-11} F, respectively: please see supplementary information S1.

3.2 Device evaluation

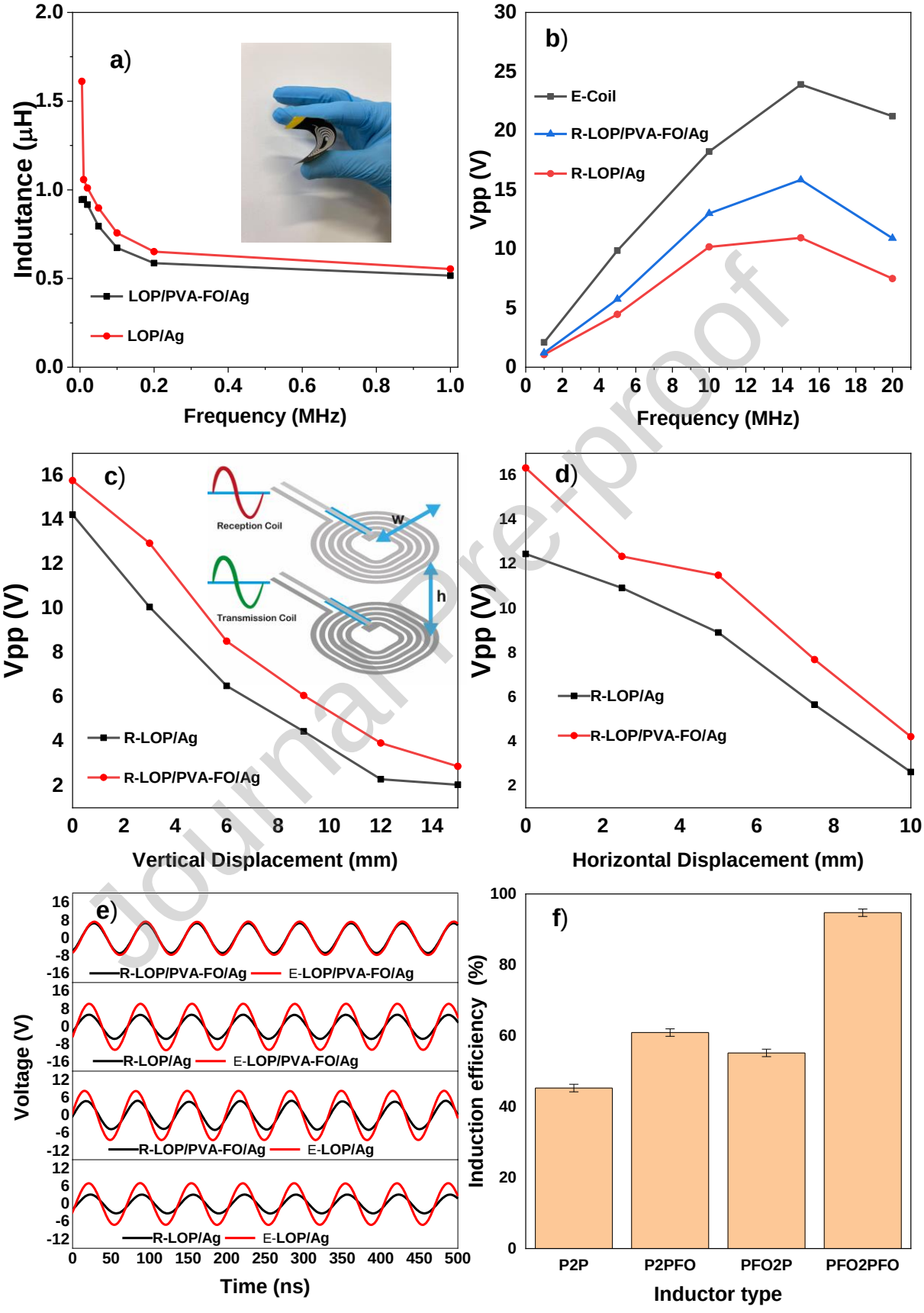

Figure 7. a) Inductance as a function of the frequency for coils printed on LOP. The inset reveals the flexibility of the developed coils. b) Relation between the peak-to-peak voltage (Vpp) of the emitted (E) signal (printed circuit board FR-4 with copper core-PCB) and the received (R) signal on coils printed on LOP. Received Vpp on coils printed on LOP as a function of the: c) vertical displacement, and d) horizontal displacement (inset of Figure 6c). e) Relation between the signals (E and R) using the coils printed on LOP (with and without PVA-FO core). f) Induction efficiency on inductors using: i) LOP/Ag materials as both emitter and receiver (P2P); ii) LOP/Ag as emitter and LOP/PVA-FO/Ag as receiver (P2PFO); iii) LOP/PVA-FO/Ag as emitter and LOP/Ag as receiver (PFO2P); and LOP/PVA-FO/Ag as both emitter and receiver (PFO2PFO). Experiments c-f have been performed at the resonance frequency of 15 kHz.

Figure 7a evidences an increase on the inductance value of ≈20% when the PVA-FO core is added to the LOP/Ag coil because of the increased magnetic permeability. **Figure 7b** shows that the resonance frequency for the energy transfer system (ETS) composed of an emission coil (PCR FR-4) and a receiver coil is ≈15 MHz at which the input and output voltage reached maximum values. Once the PVA-FO layer enhances magnetic coupling between the printed Ag coils transmitting and receiving the magnetic field[21], the receiver coil composed of LOP/PVA-FO/Ag exhibited higher Vpp (15.52 V) when compared to the LOP/Ag coil (10.36 V) which leads to induction efficiencies of 66% and 44% respectively. The enhanced magnetic coupling with the introduction of the PVA-FO layer also explains the higher efficiencies of the R-LOP/PVA-FO/Ag coil when the emitter and receiver coils were separated vertically (**Figure 7c**) and horizontally (**Figure 7d**). Additionally, the high permeability of the PVA-FO layer causes the incoming magnetic field to flow through itself and therefore prevents the magnetic field from reaching any external objects, including electronic devices or human bodies, near the coils[21].

When compared to the R-LOP/Ag coil, the R-LOP/PVA-FO/Ag exhibits induction performances 30% higher on the vertical displacement experiment and 34% higher on the horizontal displacement experiment.

The induction capability of the paper-based materials has been also tested by using only LOP-based coils with (R-LOP/PVA-FO/Ag) and without (R-LOP/Ag) magnetic layer, both as emitters and receivers (**Figure 7e**).

The device (P2P) that had both the emitter and the receiver without a PVA-FO core revealed the lowest induction efficiency (≈45%), the device (PFO2PFO) that had both the emitter and the receiver with a PVA-FO core revealed the highest induction efficiency (≈94%), and the devices with a mixed composition (one of the coils with a PVA-FO core and the other without a PVA-FO core: PFO2P and P2PFO) exhibited intermediate performances (54% and 61%).
No considerable differences were detected on the performance of the ETS after being submitted to bending such as shown in **Figure 7a** (inset): Please see supplementary information S2.

Such PFO2PFO inductor device, with an induction efficiency higher than the exhibited by some printed inductors recently reported (**Table 1**), takes advantage not only of the higher magnetic permeability but also of the successful shielding of the canceling magnetic field coming from neighboring metallic components that the 2 PVA-FO layers induced [21].

Table 1. Comparison of the induction efficiencies between recently reported printed WPTM and the one exhibited by a conventional PCB planar inductor.

Coil (conductor@core)	Substrate	Technique	Induction efficiency/distance (%/cm)	Size (length/width/line width)	Ref.
Ag@air	polyimide	direct writing	50/0	61/61/1 mm	[15]
Polyimide-Ag@ NiZn-ferrite	PDMS	inkjet	36/0	42/42/1mm	[12]
Ag@$Ni_{0.4}Zn_{0.6}O/Fe_2O_3$	silicon	inkjet	13/1.5	41/41/1 mm	[21]
Ag@PVA-FO	paper	screen	94/0; 15/1.5*	30/30/1 mm	[This]
Conventional PCB planar inductor			98/0	20/9/1 mm	[54]

*74/0 and 13/1.5 after 50 bending cycles such as the one on the inset of Figure 7 a.

Finally, the performance of the WPTM composed of 2 LOP/PVA-FO/Ag coils was confirmed with the successful powering of light-emitting diodes (LEDs): **Figure 8** and **Supplementary Video**.

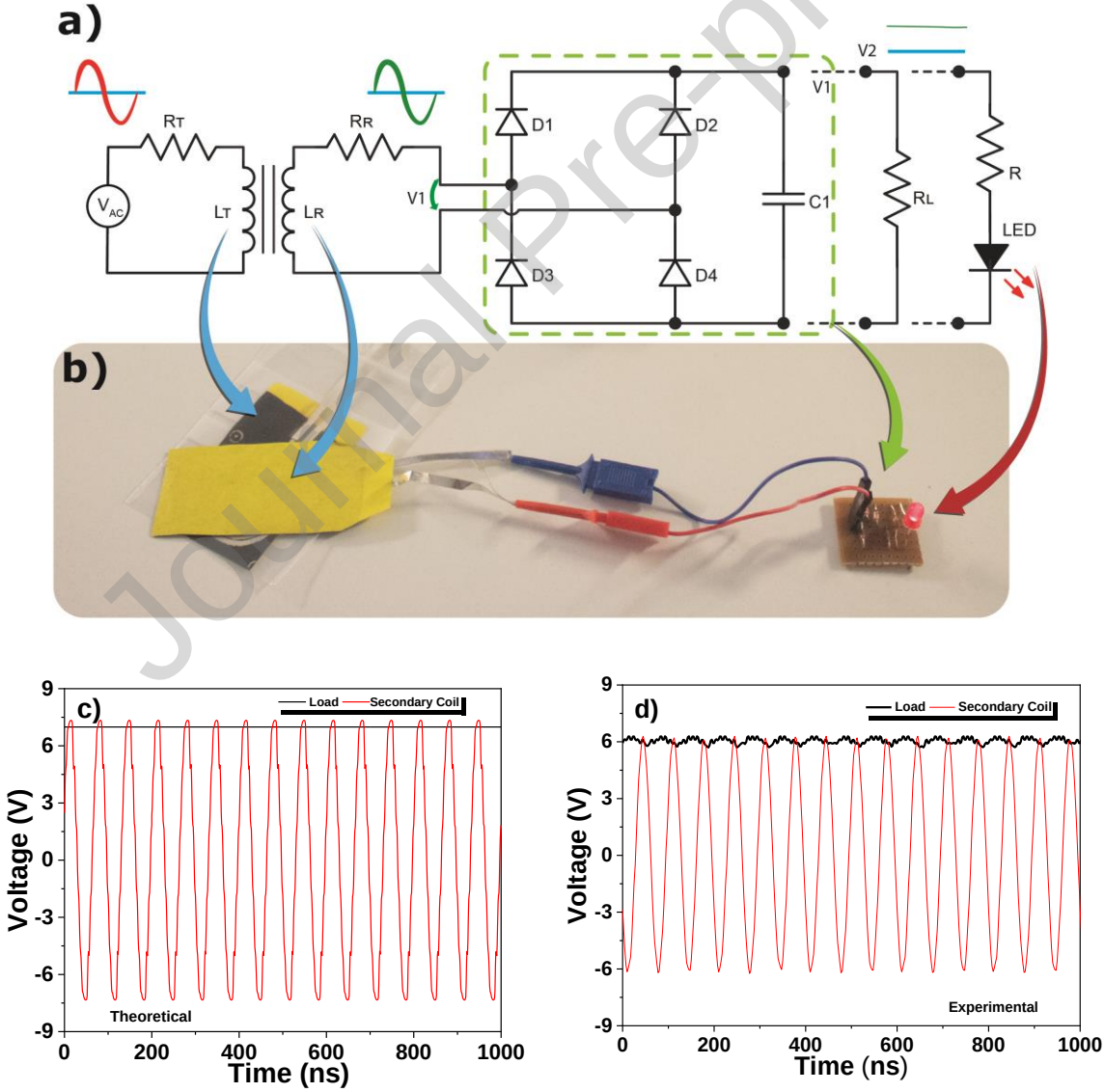

Figure 8. Induction device composed of R-LOP/PVA-FO/Ag and E-LOP/PVA-FO/Ag with a rectification circuit for powering resistive load or a LED: a) Scheme and, b) photograph. The

input on the E-LOP/PVA-FO/Ag was and AC signal of 20 Vpp provided by an Agilent 33220A. R_T and R_R= 20 Ω, LT and L_R= 0.6 µH, and c1= 100nF, R_L= 10kΩ. c) Simulation d) Experimental results of the voltage on the secondary coil (V1) and output voltage on the resistive load (V2).

Figure 8 c-d shows the simulation results of the power converter circuit using the SPICE software, Micro-cap 12, from Spectrum, and the experimental results for a resistive load of 10 kΩ. There is a good correlation between the theoretical model and experimental results for the induced voltage in the secondary coil. The experimenatl data display lower voltages (≈15%) when compared to the theretical ones as a result of losses on the circuit. Additionally, a higher ripple can be detected in the experimental data due to incomplete suppression of the alternating waveform, being increased if the load value increases as a result of the current limits of the power supply.

The same powering strategy can be used to wirelessly power small electronic devices such as security papers, interactive/smart books, smart packaging, and health care gadgets, among others [6, 55].

4. Conclusion

Paper-based coils have been fabricated by screen-printing of PVA-FO as magnetic core and Ag inks as conductive patterns on commercially available paper substrates. The paper-based coils layers exhibit good mechanical adhesion (maximum of 0.3% weight loss), hydrophobicity (117º contact angles) and inductances on the 0.5-1.7 µH range. It is also shown that the printed structures can be integrated on WPTM that exhibit induction efficiencies up to 94%. Overall, this study establishes a practical combination of advanced functional materials, printing methods and technologies to produce environmentally friendly paper-based electronic devices.

Acknowledgements

Funding: All authors thank the FCT- Fundação para a Ciência e Tecnologia the financial support in the context of the Strategic Funding UID/FIS/04650/2019 and under projects PTDC/EEI-SII/5582/2014, PTDC/BTM-MAT/28237/2017 and PTDC/EMD-EMD/28159/2017. Pedro Martins and Clarisse Ribeiro thank the FCT for the contracts under the Stimulus of Scientific Employment, Individual Support: CEECIND/03975/2017, and 2020.04163.CEECIND, respectively. Ricardo Brito-Pereira also acknowledges the FCT for the SFRH/BD/140698/2018 grant. Finally, the authors acknowledge funding by the Basque Government Industry and Education Department under the ELKARTEK, and PIBA (PIBA-2018-06) programs, respectively. Finally, funding from European Union's Horizon 2020 Program for Research, ICT-02-2018 - Flexible and Wearable Electronics, Grant agreement no. 824339 – WEARPLEX is also acknowledged.

TOC

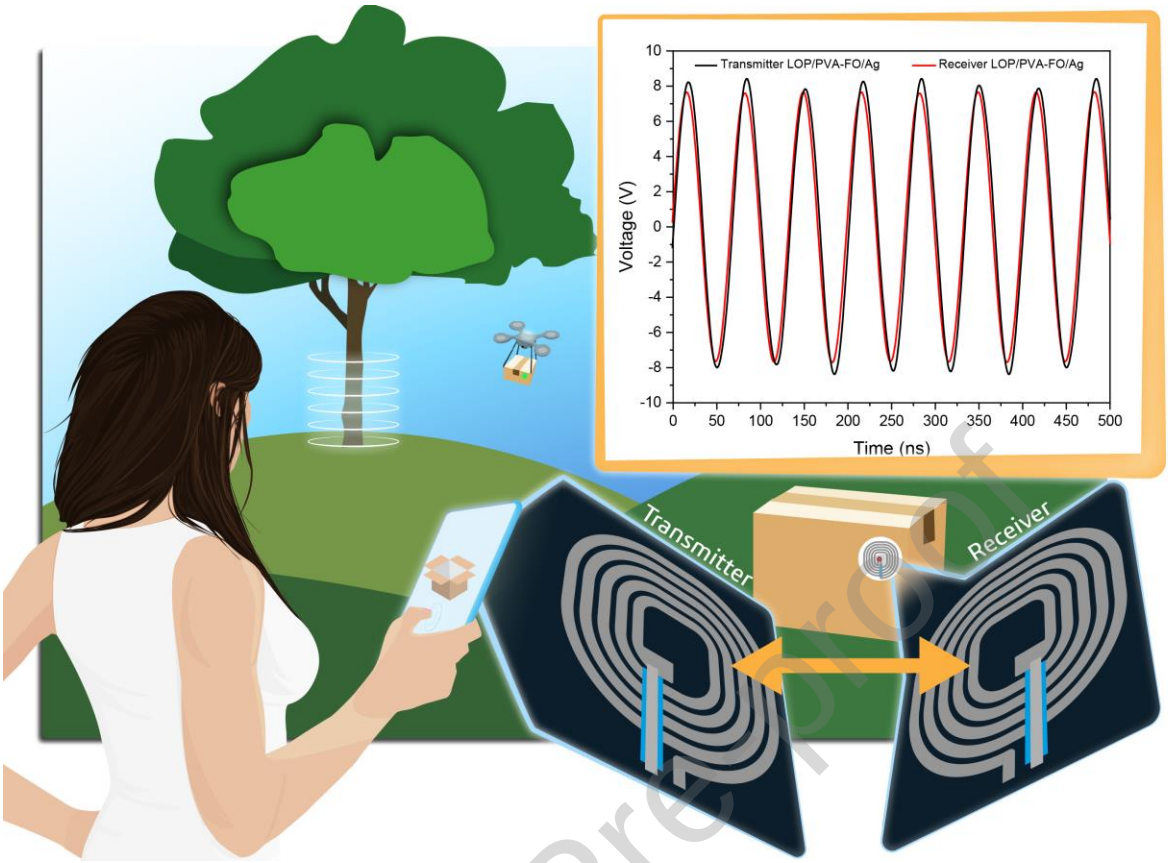

Author contributions: All authors have contributed equally to this work

Competing interests: There are no competing interests.

References

[1] E. Fortunato, N. Correia, P. Barquinha, L. Pereira, G. Goncalves, R. Martins, High-performance flexible hybrid field-effect transistors based on cellulose fiber paper, *IEEE Electron Device Letters* **2008**, *29*, 988.
[2] Z. Wang, Z. Ma, J. Sun, Y. Yan, M. Bu, Y. Huo, Y. F. Li, N. Hu, Recent advances in natural functional biopolymers and their applications of electronic skins and flexible strain sensors, *Polymers* **2021**, *13*, 1.
[3] M. Wang, T. Sun, D. Wan, M. Dai, S. Ling, J. Wang, Y. Liu, Y. Fang, S. Xu, J. Yeo, H. Yu, S. Liu, Q. Wang, J. Li, Y. Yang, Z. Fan, W. Chen, Solar-powered nanostructured biopolymer hygroscopic aerogels for atmospheric water harvesting, *Nano Energy* **2021**, *80*.
[4] J. Eun, S. Jeon, Direct fabrication of high performance moisture-driven power generators using laser induced graphitization of sodium chloride-impregnated cellulose nanofiber films, *Nano Energy* **2022**, *92*.
[5] Z. X. Chen, J. L. Li, P. Pan, P. Bao, X. Zeng, X. Z. Zhang, Combination gut microbiota modulation and chemotherapy for orthotopic colorectal cancer therapy, *Nano Today* **2021**, *41*.
[6] R. Brito-Pereira, C. R. Tubio, S. Lanceros-Mendez, P. Martins, A Facile Nanoimpregnation Method for Preparing Paper-Based Sensors and Actuators, *Advanced Materials Technologies* **2021**.

[7] G. Ferreira, A. Opinião, S. Das, S. Goswami, L. Pereira, S. Nandy, R. Martins, E. Fortunato, Smart IoT enabled interactive self-powered security tag designed with functionalized paper, *Nano Energy* **2022**, *95*.
[8] B. Pang, G. Jiang, J. Zhou, Y. Zhu, W. Cheng, D. Zhao, K. Wang, G. Xu, H. Yu, Molecular-Scale Design of Cellulose-Based Functional Materials for Flexible Electronic Devices, *Advanced Electronic Materials* **2021**, *7*.
[9] T. Su, N. Liu, Y. Gao, D. Lei, L. Wang, Z. Ren, Q. Zhang, J. Su, Z. Zhang, MXene/cellulose nanofiber-foam based high performance degradable piezoresistive sensor with greatly expanded interlayer distances, *Nano Energy* **2021**, *87*.
[10] K. E. Tomberlin, R. Venditti, Y. Yao, Life cycle carbon footprint analysis of pulp and paper grades in the united states using production-line-based data and integration, *BioResources* **2020**, *15*, 3899.
[11] J. M. Chard, L. Basson, G. Creech, D. A. Jesson, P. A. Smith, Shades of green: Life cycle assessment of a urethane methacrylate/unsaturated polyester resin system for composite materials, *Sustainability (Switzerland)* **2019**, *11*.
[12] M. Bissannagari, T. H. Kim, J. G. Yook, J. Kim, All inkjet-printed flexible wireless power transfer module: PI/Ag hybrid spiral coil built into 3D NiZn-ferrite trench structure with a resonance capacitor, *Nano Energy* **2019**, *62*, 645.
[13] Y. Zhou, H. Qi, J. Yang, Z. Bo, F. Huang, M. S. Islam, X. Lu, L. Dai, R. Amal, C. H. Wang, Z. Han, Two-birds-one-stone: Multifunctional supercapacitors beyond traditional energy storage, *Energy and Environmental Science* **2021**, *14*, 1854.
[14] N. Khossossi, W. Luo, Z. Haman, D. Singh, I. Essaoudi, A. Ainane, R. Ahuja, Revealing the superlative electrochemical properties of o-B2N2 monolayer in Lithium/Sodium-ion batteries, *Nano Energy* **2022**, *96*.
[15] M. Wagih, A. Komolafe, B. Zaghari, "Wearable Wireless Power Transfer using Direct-Write Dispenser Printed Flexible Coils", presented at *FLEPS 2020 - IEEE International Conference on Flexible and Printable Sensors and Systems*, 2020.
[16] N. Tesla, Apparatus for transmitting electrical energy, *New York, USA Patent* US37181707A Serial No. 90,245, 1907.
[17] M. Zhu, Z. Yi, B. Yang, C. Lee, Making use of nanoenergy from human – Nanogenerator and self-powered sensor enabled sustainable wireless IoT sensory systems, *Nano Today* **2021**, *36*.
[18] M. Sala de Medeiros, D. Goswami, D. Chanci, C. Moreno, R. V. Martinez, Washable, breathable, and stretchable e-textiles wirelessly powered by omniphobic silk-based coils, *Nano Energy* **2021**, *87*.
[19] C. Zhang, J. Chen, W. Xuan, S. Huang, B. You, W. Li, L. Sun, H. Jin, X. Wang, S. Dong, J. Luo, A. J. Flewitt, Z. L. Wang, Conjunction of triboelectric nanogenerator with induction coils as wireless power sources and self-powered wireless sensors, *Nature Communications* **2020**, *11*.
[20] S. Cao, H. Zhang, R. Guo, W. Zhang, S. Sang, Wireless Power Transmission Enabled by a Triboelectric Nanogenerator via a Magnetic Interaction, *Energy Technology* **2019**, *7*.
[21] M. Bissannagari, W. Lee, W. Y. Lee, J. H. Jeong, J. Kim, Fully-Inkjet-Printed Ag-Coil/NiZn-Ferrite for Flexible Wireless Power Transfer Module: Rigid Sintered Ceramic Body into Flexible Form, *Advanced Functional Materials* **2017**, *27*.
[22] L. Jiang, G. Lu, Y. Yang, Y. Xu, F. Qi, J. Li, B. Zhu, Y. Chen, Multichannel Piezo-Ultrasound Implant with Hybrid Waterborne Acoustic Metastructure for Selective Wireless Energy Transfer at Megahertz Frequencies, *Advanced Materials* **2021**, *33*.
[23] H. E. Lee, J. Choi, S. H. Lee, M. Jeong, J. H. Shin, D. J. Joe, D. Kim, C. W. Kim, J. H. Park, J. H. Lee, D. Kim, C. S. Shin, K. J. Lee, Monolithic Flexible Vertical GaN Light-Emitting Diodes for a Transparent Wireless Brain Optical Stimulator, *Advanced Materials* **2018**, *30*.

[24] A. Chandrasekhar, N. R. Alluri, M. S. P. Sudhakaran, Y. S. Mok, S. J. Kim, A smart mobile pouch as a biomechanical energy harvester towards self-powered smart wireless power transfer applications, *Nanoscale* **2017**, *9*, 9818.
[25] D. Helena, A. Ramos, T. Varum, J. N. Matos, The use of 3d printing technology for manufacturing metal antennas in the 5g/iot context, *Sensors* **2021**, *21*.
[26] R. Brito-Pereira, C. Ribeiro, N. Pereira, S. Lanceros-Mendez, P. Martins, Printed multifunctional magnetically activated energy harvester with sensing capabilities, *Nano Energy* **2022**, *94*, 106885.
[27] T. Leng, K. Pan, Y. Zhang, J. Li, S. Afroj, K. S. Novoselov, Z. Hu, Screen-Printed Graphite Nanoplate Conductive Ink for Machine Learning Enabled Wireless Radiofrequency-Identification Sensors, *ACS Applied Nano Materials* **2019**, *2*, 6197.
[28] X. Zhu, M. Liu, X. Qi, H. Li, Y. F. Zhang, Z. Li, Z. Peng, J. Yang, L. Qian, Q. Xu, N. Gou, J. He, D. Li, H. Lan, Templateless, Plating-Free Fabrication of Flexible Transparent Electrodes with Embedded Silver Mesh by Electric-Field-Driven Microscale 3D Printing and Hybrid Hot Embossing, *Advanced Materials* **2021**, *33*.
[29] M. Idrees, S. Batool, J. Cao, M. S. Javed, S. Xiong, C. Liu, Z. Chen, 3D printed PC/SiOC@Zn hybrid composite as dendrite-free anode for Zn-Ion battery, *Nano Energy* **2022**, *100*.
[30] N. Zavanelli, W. H. Yeo, Advances in Screen Printing of Conductive Nanomaterials for Stretchable Electronics, *ACS Omega* **2021**, *6*, 9344.
[31] G. Zhu, P. Ren, J. Yang, J. Hu, Z. Dai, H. Chen, Y. Li, Z. Li, Self-powered and multi-mode flexible sensing film with patterned conductive network for wireless monitoring in healthcare, *Nano Energy* **2022**, *98*.
[32] V. Kokol, V. Vivod, Z. Peršin, T. Kamppuri, P. Dobnik-Dubrovski, Screen-printing of microfibrillated cellulose for an improved moisture management, strength and abrasion resistant properties of flame-resistant fabrics, *Cellulose* **2021**, *28*, 6663.
[33] W. He, H. Wang, Y. Huang, T. He, F. Chi, H. Cheng, D. Liu, L. Dai, L. Qu, Textile-based moisture power generator with dual asymmetric structure and high flexibility for wearable applications, *Nano Energy* **2022**, *95*.
[34] C. Xiong, M. Li, Q. Han, W. Zhao, L. Dai, Y. Ni, Screen printing fabricating patterned and customized full paper-based energy storage devices with excellent photothermal, self-healing, high energy density and good electromagnetic shielding performances, *Journal of Materials Science and Technology* **2022**, *97*, 190.
[35] V. Rajendran, A. M. V. Mohan, M. Jayaraman, T. Nakagawa, All-printed, interdigitated, freestanding serpentine interconnects based flexible solid state supercapacitor for self powered wearable electronics, *Nano Energy* **2019**, *65*.
[36] B. F. Gonçalves, J. Oliveira, P. Costa, V. Correia, P. Martins, G. Botelho, S. Lanceros-Mendez, Development of water-based printable piezoresistive sensors for large strain applications, *Composites Part B: Engineering* **2017**, *112*, 344.
[37] M. R. Havstad, Chapter 5 - Biodegradable plastics in *Plastic Waste and Recycling*, (Ed: T. M. Letcher), Academic Press, 2020, 97.
[38] X. Chen, W. Li, S. Hu, N. G. Akhmedov, D. Reed, X. Li, X. Liu, Polyvinyl alcohol coating induced preferred crystallographic orientation in aqueous zinc battery anodes, *Nano Energy* **2022**, *98*.
[39] T.-Y. Liu, S.-H. Hu, K.-H. Liu, D.-M. Liu, S.-Y. Chen, Study on controlled drug permeation of magnetic-sensitive ferrogels: Effect of Fe3O4 and PVA, *Journal of Controlled Release* **2008**, *126*, 228.
[40] A. Bahadur, A. Saeed, M. Shoaib, S. Iqbal, M. I. Bashir, M. Waqas, M. N. Hussain, N. Abbas, Eco-friendly synthesis of magnetite (Fe3O4) nanoparticles with tunable size: Dielectric, magnetic, thermal and optical studies, *Materials Chemistry and Physics* **2017**, *198*, 229.

[41] W. Qing, Z. Hu, Q. Ma, W. Zhang, Conductive Fe3O4/PANI@PTFE membrane for high thermal efficiency in interfacial induction heating membrane distillation, *Nano Energy* **2021**, *89*.
[42] B. Plovie, Y. Yang, J. Guillaume, S. Dunphy, K. Dhaenens, S. Van Put, B. Vandecasteele, T. Vervust, F. Bossuyt, J. Vanfleteren, Arbitrarily Shaped 2.5D Circuits using Stretchable Interconnects Embedded in Thermoplastic Polymers, *Advanced Engineering Materials* **2017**, *19*.
[43] Z. L. Chen, P. Y. Chao, S. H. Chiu, Empirical viscosity model for polymers with power-law flow behavior, *Journal of Applied Polymer Science* **2003**, *88*, 3045.
[44] T. Hao, S. Wang, H. Xu, X. Zhang, J. Xue, S. Liu, Y. Song, Y. Li, J. Zhao, Highly robust, transparent, and conductive films based on AgNW-C nanowires for flexible smart windows, *Applied Surface Science* **2021**, *559*.
[45] M. Han, J. M. Kim, H. Sohn, "Dual-mode wireless power transfer module for smartphone application", presented at *IEEE Antennas and Propagation Society, AP-S International Symposium (Digest)*, 2015.
[46] B. E. Rapp, Chapter 9 - Fluids in *Microfluidics: Modelling, Mechanics and Mathematics*, (Ed: B. E. Rapp), Elsevier, Oxford 2017, 243.
[47] S. Krainer, C. Smit, U. Hirn, The effect of viscosity and surface tension on inkjet printed picoliter dots, *RSC Advances* **2019**, *9*, 31708.
[48] B. He, S. Yang, Z. Qin, B. Wen, C. Zhang, The roles of wettability and surface tension in droplet formation during inkjet printing, *Scientific Reports* **2017**, *7*.
[49] A. Matavž, V. Bobnar, B. Malič, Tailoring Ink-Substrate Interactions via Thin Polymeric Layers for High-Resolution Printing, *Langmuir* **2017**, *33*, 11893.
[50] S. Some, Y. Xu, Y. Kim, Y. Yoon, H. Qin, A. Kulkarni, T. Kim, H. Lee, Highly sensitive and selective gas sensor using hydrophilic and hydrophobic graphenes, *Scientific Reports* **2013**, *3*.
[51] A. R. K. Sasikala, V. K. Kaliannagounder, N. R. Alluri, B. K. Shrestha, S. J. Kim, H. Ali-Boucetta, C. H. Park, A. R. Unnithan, Development of self-powered multifunctional piezomagnetic nanoparticles for non-invasive post-surgical osteosarcoma theranogeneration, *Nano Energy* **2022**, *96*.
[52] S. Kopacic, A. Walzl, A. Zankel, E. Leitner, W. Bauer, Alginate and chitosan as a functional barrier for paper-based packaging materials, *Coatings* **2018**, *8*.
[53] B. Barari, T. K. Ellingham, I. I. Ghamhia, K. M. Pillai, R. El-Hajjar, L. S. Turng, R. Sabo, Mechanical characterization of scalable cellulose nano-fiber based composites made using liquid composite molding process, *Composites Part B: Engineering* **2016**, *84*, 277.
[54] Z. Yu, X. Yang, G. Wei, L. Wang, K. Wang, W. Chen, J. Wei, A Novel High-Current Planar Inductor with Cooling Fins Based on 3D Printing, *IEEE Transactions on Power Electronics* **2021**.
[55] T. Zhu, Y. Yang, Y. Liu, R. Lopez-Hallman, Z. Ma, L. Liu, X. Gong, Wireless portable light-weight self-charging power packs by perovskite-organic tandem solar cells integrated with solid-state asymmetric supercapacitors, *Nano Energy* **2020**, *78*.

Authors' biosketch

Ricardo Brito Pereira is graduated in Biomedical Engineering and at the moment is a PhD student at Universidade do Minho. His work is focused on using printing techniques for advanced applications and in developing a new generation of point of care devices using polymer-based smart materials. Following the willing to evolve, he already worked as visiting scientist in several institutions as the Boston University (USA), Karlsruhe Institute of Technology (Germany), Leonardino Srl (Italy) or Basque Centre for Materials (Spain). He is also involved in some biotechnological entrepreneurship projects.

Clarisse Ribeiro graduated in Biomedical Engineering (master in Electronic Medicine) in 2008, receiving PhD in Physics in 2012 (both at University of Minho, Portugal). She is an assistant researcher at the Center of Physics of University of Minho, integrating the «Functional and smart materials and surfaces for advanced applications» line. She possess expertise in the area of interface between biomaterials/nanostructured materials and cell types and tissues, smart scaffold processing and cell culture for active tissue engineering with leading publications and innovation. Furthermore, she presents expertise in novel bioreactors design/implementation taking advantage of the developed materials to create suitable cell microenvironments.

Nelson Pereira received his graduation and master in Industrial Electronics Engineering and Computers at the University of Minho, Braga, Portugal. He is presently a Ph.D grant holder at University of Minho on the Electroactive Smart Material Group (ESM), Portugal. His work aims to explore, develop and incorporate new smart and functional printed materials (such as transparent conductive inks and electroactive materials) in order to implement new interactive platforms.

S. Lanceros-Mendez is Ikerbasque Professor at BCMaterials, Basque Center for Materials, Applications and Nanostructures, Leioa, Spain, where he is the Scientific Director. He is Associate Professor at the Physics Department of the University of Minho, Portugal (on leave), where also belongs to the Center of Physics. He graduated in Physics at the University of the Basque Country, Leioa, Spain and obtained his Ph.D. degree at the Institute of Physics of the Julius-Maximilians-Universität Würzburg, Germany. His work is focused in the development of smart and multifunctional materials for sensors and actuators, energy and biomedical applications.

Pedro Martins graduated in Physics and Chemistry in 2006, receiving the Ph.D degree in Physics in 2012, from the University of Minho (Braga, Portugal) in collaboration with Basque Country University (Spain) and Cambridge University (UK). In 2013-2014 he was also researcher at the International Iberian Nanotechnology Laboratory (Portugal). He is Assistant Researcher in the Physics Center of the University of Minho, and his work is focused on polymer-based magnetoelectric materials, printed magnetics, spintronics, and multifunctional polymers for advanced applications.

Declaration of interests

☒ The authors declare that they have no known competing financial interests or personal relationships that could have appeared to influence the work reported in this paper.

☐The authors declare the following financial interests/personal relationships which may be considered as potential competing interests:

CRediT authorship contribution statement

R. Brito-Pereira: Conceptualization, Methodology, Validation, Investigation, Writing - Original Draft, Visualization
C. Ribeiro: Methodology, Validation, Investigation, Writing - Review & Editing, Visualization, Resources
N. Pereira: Validation, Investigation, Software, Writing - Original Draft
S. Lanceros-Mendez: Methodology, Writing - Review & Editing, Resources, Supervision, Project administration, Funding acquisition
P. Martins: Conceptualization, Methodology, Validation, Investigation, Writing - Original Draft, Writing - Review & Editing, Visualization, Formal analysis, Resources, Supervision, Project administration, Funding acquisition

Highlights

- A new nanoroute for developing wireless power transfer modules (WPTM) is proposed
- It was obtained an induction efficiency of 75% (the highest reported in literature)
- This route allows the scalable production of sustainable flexible smart energy-related devices